Search for cosmic neutrinos with ANTARES

Bogazzi, C.

1. Cosmic rays and neutrino astronomy

Okay, the unexpected I can deal with...
as long as I'm expecting it, that is...

Peter Parker

This chapter focuses on cosmic rays and their connection to neutrinos. It is likely that neutrinos are created by the interactions of accelerated protons and nuclei near their sources. Being neutral particles, neutrinos are not deflected by the galactic magnetic fields. Thus, detecting astrophysical neutrinos could help to identify the source of cosmic rays.

The chapter is divided in three sections: Section 1.1 will briefly discuss the main properties of cosmic rays and the mechanism thought to be responsible for their acceleration. Section 1.2 will introduce neutrino astronomy with particular attention to neutrino production from cosmic rays. Potential cosmic rays and neutrinos sources will be presented in Section 1.3.

1.1. Cosmic rays

Cosmic rays (CRs) are energetic particles, which continuously hit the Earth's atmosphere. Primary CRs mainly consist of ionised nuclei such as protons ($\sim 85\%$), helium ($\sim 12\%$) and heavier nuclei ($\sim 1\%$) [3]. The remaining component includes electrons.

1.1.1. Flux and energy spectrum

The differential flux of cosmic rays, shown in Figure 1.1, spans many orders of magnitude in energy and it is roughly described by a broken power-law formula

$$\frac{dN}{dE} \propto E^{-\gamma}, \tag{1.1}$$

where E is the energy of the primary particle and γ is called the spectral index. The spectral index has a value of about 2.7 below $E \simeq 4 \times 10^{15}$ eV. At this energy, the "knee", the spectral index changes to 3.3. At higher energies, $E \sim 3 \times 10^{18}$ eV, it changes again to 2.6 resulting in a concave shape of the spectrum curve, the so called "ankle".

Two possible scenarios explain the steepening of the flux around the knee region:

- In the first case, the knee is explained as a consequence of the limited spatial extension and magnetic field of the source accelerator. Since the energy of the cosmic

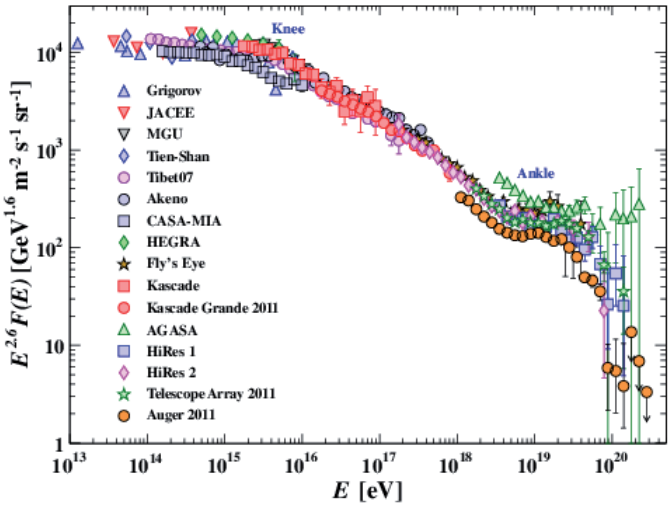

Figure 1.1.: All-particle cosmic rays energy spectrum [4]

rays is proportional to the charge of the particle, and the maximum energy the cosmic rays can be accelerated is determined by the size of the source, the size of the accelerating region has to be larger than the Larmor radius of the particle

$$r_L = 1.08 \frac{E/\mathrm{PeV}}{\mathrm{Z} \cdot \mathrm{B}/\mu\mathrm{G}} \,\mathrm{pc}, \tag{1.2}$$

where E is the energy of the particle with charge Z and B is the magnetic field of the source.

- The second scenario supposes that the galactic magnetic field is too weak to confine particles with energy above the knee. That is, the Larmor radius of a particle exceeds the thickness of the galactic disk and cosmic rays can escape the boundary of the Milky Way. Since the Larmor radius scales with E/Z, heavier nuclei can be kept inside our Galaxy up to higher energies compared to protons. Measurements on the cosmic ray composition could verify this theory.

The flattening of the energy spectrum at the ankle is generally explained as a transition from a Galactic to an extragalactic component [5]. Hence, the ankle is the energy at which the two components give an equal contribution to the particle flux. Cosmic rays above this energy are usually called Ultra-High-Energy Cosmic Rays (UHECR). Another possible interpretation is that the dip structure around the ankle region of the spectrum is

a consequence of the energy losses of protons interacting with the 2.7 K Cosmic Microwave Background (CMB)[6] via $\gamma + \mathrm{p} \rightarrow \mathrm{e}^+ + \mathrm{e}^- + \mathrm{p}$.

At the high-energy end of the spectrum the flux is suppressed. This is due to the so called Greisen-Zatsepsin-Kuz'min (GZK) effect [7, 8] which predicts that above 60 EeV protons lose energy by interacting with the CMB via pion production:

$$\begin{aligned} p + \gamma &\rightarrow \Delta^+(1232) \rightarrow p + \pi^0 \\ p + \gamma &\rightarrow \Delta^+(1232) \rightarrow n + \pi^+. \end{aligned} \tag{1.3}$$

1.1.2. Anisotropy of arrival directions

The presence of anisotropies in the arrival direction of high-energy cosmic rays on different angular scales may help to understand their propagation and deflection as well as to identify their sources.

The distribution of the arrival direction of cosmic rays with energies below 1 EeV is uniform because of the diffusion in the galactic magnetic field. Above this energy the galactic magnetic field is too weak to significantly deflect the cosmic rays and therefore the arrival directions of cosmic rays should point back to their sources[1]. As a consequence, assuming that the sources are not uniformly distributed, an anisotropic arrival direction distribution is expected for the most energetic cosmic rays.

The Pierre Auger Collaboration reported [10] in 2010 interesting results which showed a hint of correlation between the arrival directions of 69 events observed with energies above 57 EeV and the locations of Active Galactic Nuclei (AGN) with redshift $z \leq 0.018$ (distances ≤ 75 Mpc) within an opening angle of 3.1°. A fraction of 38% of these events is correlated with AGNs. This number has to be compared with the 21% expected if the cosmic rays flux were isotropic. Figure 1.2 shows the sky map in galactic coordinates of the 69 arrival directions of CRs together with the positions of 318 AGNs.

The center of the region which shows the largest excess of arrival directions among the 69 CRs above the isotropic expectation is only 4° away from the position of the AGN Centaurus A (see also Section 1.3.3). Figure 1.3 shows the number of events as a function of the cumulative angular distance Ψ_{CenA} from the direction of Centaurus A: 12 events are within 13° from the center of the AGN with an isotropic expectation of 1.7.

With more statistics it will be possible to tell if Centaurus A is the first UHECR source to be revealed. At lower energies where the distribution of cosmic rays is expected to be uniform, the identification of a source of origin is possible only with the detection of neutrinos. Centaurus A is also one of the candidate neutrino sources considered in this thesis. According to Cuoco and Hannestad [11] an event rate of 0.5 yr^{-1} is expected for a km^3 neutrino telescope.

1.1.3. Acceleration mechanism

The mechanism most widely considered to be responsible for accelerating CRs was proposed by Enrico Fermi in 1949 [12]. Fermi considered the interactions between CRs and

[1] A typical angular resolution for a surface array detector is around 1 degree, while hybrid detector can achieve a better pointing accuracy [9]

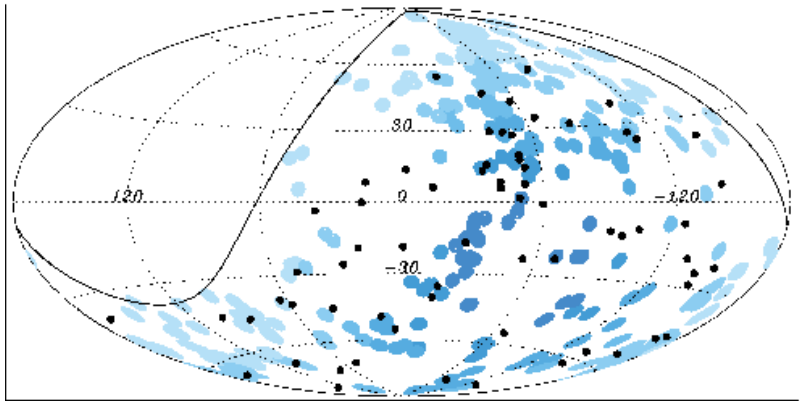

Figure 1.2.: Sky map in galactic coordinates of the 69 arrival directions of CRs with energy $E \geq 55$ EeV detected by the PAO up to December 2009 (black dots). Blue circles of radius 3.1° show the locations of the 318 selected AGNs within 75 Mpc. The darker is the blue the larger is the relative exposure. The solid line represents the field of view of the PAO for zenith angles smaller than 60°. The figure is taken from [10].

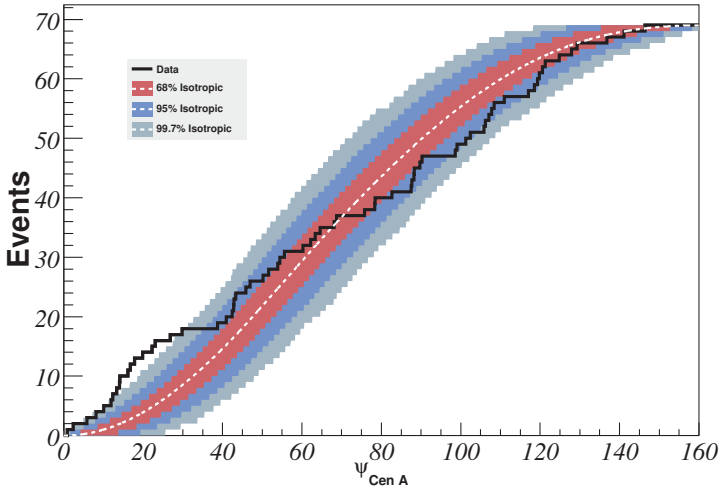

Figure 1.3.: Cumulative number of events as a function of the angular distance from the location of Centaurus A. The bands correspond to the 1σ, 2σ and 3σ confidence level (CL) for an expected isotropic flux. 13 arrival directions are within 18° from Centaurus A. Figure taken from [10].

interstellar magnetic clouds of plasma as responsible for the acceleration. A particle with initial energy E_1 enters a moving gas cloud where it is diffused by irregularities in the magnetic field. After a few deflections the particle emerges from the cloud in a random direction with energy E_2 (see the top illustration of Figure 1.4). In the rest frame of the moving cloud, the cosmic ray particle has total energy

$$E_1' = \gamma E_1(1 - \beta\cos\theta_1) = E_2', \tag{1.4}$$

with γ the Lorentz factor and $\beta = V/c$ the velocity of the cloud with respect to the laboratory frame (outside the cloud). The last equality is obtained by imposing energy conservation (the interactions between the particle and the magnetic field are elastic). The quantities with primes correspond to a frame moving with velocity V. Transforming to the laboratory frame gives:

$$E_2 = \gamma E_2'(1 + \beta\cos\theta_2'). \tag{1.5}$$

The change in energy in the laboratory frame is:

$$\frac{\Delta E}{E_1} = \frac{(E_2 - E_1)}{E_1} = \frac{1 - \beta\cos\theta_1 + \beta\cos\theta_2' - \beta^2\cos\theta_1 - \beta^2\cos\theta_1\cos\theta_2'}{1 - \beta^2} - 1. \tag{1.6}$$

The cosmic ray particle comes out from the cloud with random direction, thus $\langle\cos\theta_2'\rangle = 0$. The average value of $\cos\theta_1$ depends on the collision rate of cosmic rays with clouds for different angles so that the probability of a collision is proportional to the relative velocity between the cloud and the particle. Hence, $\langle\cos\theta_1\rangle = -V/3c$. The change in energy can now be written as:

$$\frac{\langle\Delta E\rangle}{E} = \frac{1 + \beta^2/3}{1 - \beta^2} \simeq \frac{4}{3}\beta^2. \tag{1.7}$$

From Equation 1.7 we conclude that $\langle\Delta E\rangle/E$ is positive (the particle gains energy) and is proportional to the square of beta. If $\beta << 1$ then the average energy gain per collision is very small. This is the so called 2nd order Fermi mechanism.

Fermi's theory has been extended in the 1970's (see [13] or [14] for more details) to describe a more efficient acceleration especially in the non-relativistic limit ($\beta << 1$). In this case the idea is that CR particles gain energy by bouncing back and forth over a shock fron such as the one emitted during a supernova explosion. On both sides of the shock the particles are elastically scattered off irregularities in the magnetic field.

To describe the model we consider for simplicity non-relativistic planar shocks. As illustrated in Figure 1.4 (bottom), we assume that a planar shock wave is moving with velocity $\vec{v}_s$ in the laboratory frame (region of unshocked material). V is now the velocity of the shocked material (downstream) relative to the unshocked material (upstream) and is related to the shock velocity by the relation

$$V = \frac{3}{4}v_s. \tag{1.8}$$

Equation 1.6 is also valid for this case. The main difference with the 2nd order Fermi acceleration comes from the angular average since particles can only exit planar shock

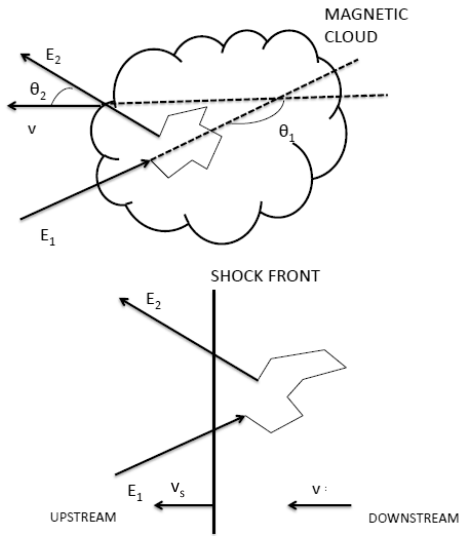

Figure 1.4.: Illustration of the second (top) and first (bottom) Fermi mechanism

fronts through the shock front. In this case $\langle \cos\theta_2' \rangle = 2/3$ and $\langle \cos\theta_1 \rangle = -2/3$. Thus

$$\frac{\langle \Delta E \rangle}{E} = \frac{1 + \frac{4}{3}\beta + \frac{4}{9}\beta^2}{1 - \beta^2} \simeq \frac{4}{3}\beta = \frac{v_s}{c}. \tag{1.9}$$

The average energy gain is now linear in β (1st order Fermi mechanism) therefore more efficient.

Another aspect which makes the 1st order Fermi mechanism a good candidate to describe CRs acceleration is the prediction of a power law flux with spectral index $\gamma = 2$ while from the 2nd order Fermi mechanism a prediction over the spectral index is impossible since it strictly depends on many parameters of the magnetic clouds.

1.2. Neutrino astronomy

On the night of February 23rd, 1987 in the Andes Mountains in Chile Ian Shelton, a research assistant at the University of Toronto pointed the big telescope of the Las Campanas observatory towards the Large Magellanic Cloud (LCM). He was looking for variable stars and novae. After three hours, as soon as the plates he was working on were developed he noticed a bright star of about 5th magnitude. The interesting thing was that, in that specific part of the sky, there should not have been any. At about the same time, Oscar Duhalde, another Las Campanas astronomer, was taking a break outside and noticed a new star in the LCM. Shelton and Duhalde were the first ones to discover the supernova SN1987A, perhaps the best-studied supernova in human history.

One of the first surprise of this supernova was its progenitor. Many models described red supergiant massive stars as typical progenitor for Type II supernova like SN1987A. However, the progenitor star of SN1987A was the blue supergiant Sanduleak -69° 202 with a mass of about $18M_{\odot}$, i.e. a relatively young and small star.

Following the suggestion of Bahcall, Dar and Piran [15], scientists from the Kamiokande II collaboration [16] looked for a possible a neutrino signal in their data. The result [17] opened a new window on the universe: a burst of 12 neutrino events was detected at 7h 35m 35s UT on February 23, two hours before the first optical light was recorded. Similar results (see [18, 19]) were obtained by the IMB [20] (8 events) and Baksan [21] (5 events) experiments. The observation of these events provided an unique opportunity to investigate the dynamics of supernova explosions [22].

Figure 1.5 shows the predicted astrophysical neutrino energy spectrum. It covers 15 orders of magnitude in energy and 42 in intensity of the flux. The analysis presented in this thesis is sensitive to neutrinos in the energy range 100 GeV - 100 TeV. In the following sections we discuss the main sources of astrophysical neutrinos from the low energy cosmic neutrino background to the high-energies.

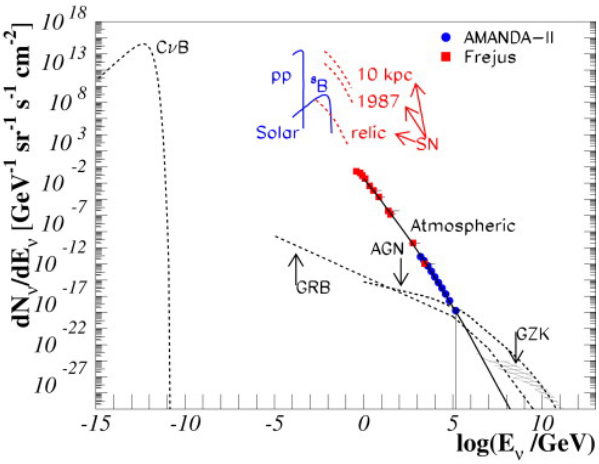

Figure 1.5.: Neutrino spectrum for several source predictions. The flux predicted from point sources have been scaled to $1/(4\pi)$ in order to be comparable with diffuse spectra. The atmospheric neutrino data are from the FREJUS (red squares) and AMANDA (blue circles) experiment. Figure taken from [23].

1.2.1. Cosmic neutrino background

The Cosmic Neutrino Background (CνB) is the neutrino equivalent of the Cosmic Microwave Background. It is a relic of the big bang which decoupled from matter when the universe was roughly 1 second old and had a temperature of about 1 MeV. Direct detection of the CνB represents a big challenge.

1.2.2. Solar neutrinos

The first identified source of extraterrestrial neutrinos is the Sun. Solar neutrinos are produced by the nuclear reactions that power the Sun such as the proton-proton (pp) chain and the CN-NO bi-cycle. The pp chain can be summarised by the reaction

$$4p \rightarrow {}^4He + 2e^+ + 2\nu_e, \tag{1.10}$$

with an average neutrino energy of $\langle E_\nu \rangle \sim 0.6$ MeV. The CN-NO bi-cycle also converts hydrogen to helium but involves heavier nuclei like carbon, nitrogen and oxygen. The energy spectrum of solar neutrinos is shown in Figure 1.6.

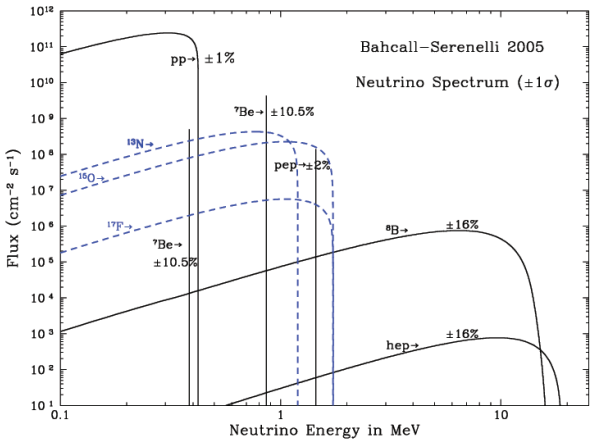

Figure 1.6.: Energy spectrum for solar neutrinos predicted by the standard solar model. Black solid lines show the neutrino flux from reactions of the pp chain, while blue lines correspond to the CN-NO bi-cycle. Figure taken from [4].

Following the idea to use chlorine as medium to detect neutrinos suggested by Bruno Pontecorvo in 1946 [26], the first experiment to detect solar neutrinos was built in the Homestake gold mine in South Dakota in 1968. The neutrino absorption reaction used was:

$$\nu_e + {}^{37}\mathrm{Cl} \rightarrow \mathrm{e}^- + {}^{37}\mathrm{Ar}. \tag{1.11}$$

The energy threshold for this reaction is 0.814 MeV.

The first results from the Homestake detector showed a deficit of neutrinos. The rate of detected neutrinos was roughly 2.5 Solar Neutrino Units (SNU)[2] over an expected capture rate of 7.6 SNU. This discrepancy, known as Solar Neutrino Problem, remained unresolved for many years and was also confirmed by other experiments such as Kamiokande (and its successor Super Kamiokande) [16] and Gallex [27].

[2] A Solar Neutrino Unit is defined as the product of neutrino flux and the neutrino cross section. 1 SNU corresponds to 10^{-36} captures per target per atom per second.

The final answer to this dilemma came from Sudbury Neutrino Observatory (SNO) experiment [28]. The SNO experiment was able to detect the total flux of solar neutrinos of any flavor. In 2002, the SNO collaboration reported their results. The sum of all the fluxes for all the three flavors was consistent with the predicted electron neutrino flux. It was a confirmation of the observation of neutrino flavor oscillations already announced by Super-Kamiokande in 1998 [3] and the solar neutrino model.

1.2.3. High-energy astrophysical neutrinos

The production of high-energy neutrinos is expected by the interactions of accelerated cosmic rays with dense matter or photons field near the cosmic ray source. The dominant channels near the π production threshold for nucleon-photon interactions are

$$\begin{aligned} p + \gamma &\to \Delta^+ \to \pi^0 + p \\ p + \gamma &\to \Delta^+ \to \pi^+ + n. \end{aligned} \tag{1.12}$$

$$\begin{aligned} n + \gamma &\to \Delta^0 \to \pi^0 + n \\ n + \gamma &\to \Delta^0 \to \pi^- + p. \end{aligned} \tag{1.13}$$

Pions are also generated in nucleon-nucleon processes, such as:

$$\begin{aligned} p + p &\to p + p + \pi^0 \\ &\to p + n + \pi^+ \end{aligned} \tag{1.14}$$

$$\begin{aligned} p + n &\to p + n + \pi^0 \\ &\to p + p + \pi^-. \end{aligned} \tag{1.15}$$

The charged pions decay into neutrinos while the neutral pions decay into gamma rays:

$$\begin{aligned} &\pi^0 \to \gamma + \gamma \\ &\pi^+ \to \mu^+ + \nu_\mu \to e^+ + \nu_e + \bar{\nu}_\mu + \nu_\mu \\ &\pi^- \to \mu^- + \bar{\nu}_\mu \to e^- + \bar{\nu}_e + \nu_\mu + \bar{\nu}. \end{aligned} \tag{1.16}$$

At higher energies kaons can be produced which also decay into neutrinos. The four leptons emerging from the decay of the pion carry roughly the same fraction of the energy. As a consequence, each neutrino carries about $1/4$ of the pion's initial energy. Since for high-energy protons roughly 20% of the initial energy, E_p, is transferred to the pion, we obtain for the neutrino energy, E_ν, that $E_\nu = E_p/20$.

The flavor ratio[4] at the source is

$$\nu_e : \nu_\mu : \nu_\tau = 1 : 2 : 0. \tag{1.17}$$

[3] The fact that if neutrinos have non-zero masses, they could oscillate between flavors was first suggested by Bruno Pontecorvo in the 1950s.

[4] we do not make any distinction between neutrinos and anti-neutrinos

	π^+	π^0	ν_μ	γ	$x_{\nu/\gamma}$
p-p	$\frac{1}{3}$	$\frac{1}{3}$	$2{\cdot}\frac{1}{2}\cdot\frac{1}{4}\cdot\frac{1}{3}=\frac{1}{6}$	$\frac{1}{2}\cdot\frac{1}{3}=\frac{1}{6}$	1
	π^+/π^0	p/n	ν_μ	γ	$x_{\nu/\gamma}$
p-γ	$\frac{1}{3}$	$\frac{2}{3}$	$\frac{1}{2}\cdot\frac{1}{3}=\frac{1}{6}$	$2{\cdot}\frac{2}{3}\cdot\frac{1}{2}=\frac{2}{3}$	4

Table 1.1.: Fraction of the proton energy which goes to pions, muon neutrinos and photons in p-p and p-γ interactions.

Taking into account flavor oscillations, the resulting flavor ratio at Earth is approximately:

$$\nu_e : \nu_\mu : \nu_\tau \approx 1 : 1 : 1. \tag{1.18}$$

In case of sources with high magnetic fields the contribution from muon decay could be suppressed due to the loss energy by mesons and/or muons. The observed flavor ratio is then [30]:

$$\nu_e : \nu_\mu : \nu_\tau \approx 1 : 1.8 : 1.8. \tag{1.19}$$

Normalisation of the flux

In the discussed hadronic processes, both TeV photons and neutrinos are produced by the decay of neutral and charged pions respectively. Thus, it is possible to relate gamma-ray and neutrino fluxes by imposing simple energy conservation as [23, 24]:

$$\int_{E_\gamma^{\min}} \frac{dN_\gamma}{dE_\gamma} E_\gamma dE_\gamma = x_{\nu/\gamma} \cdot \int_{E_\nu^{\min}} \frac{dN_\nu}{dE_\nu} E_\nu dE_\nu, \tag{1.20}$$

where $E_\gamma^{\min}$ is the minimum energy of the photons with hadronic origin and $E_\nu^{\min}$ the minimum energy of the neutrinos. The constant of proportionality $x_{\nu/\gamma}$ depends on whether the neutral pions are of pp or $p\gamma$ origin and in particular on the fraction of energy which goes into pion production. In pp interactions 1/3 of the proton energy goes into each pion flavor on average. The charged pion then decays into muons which decay into electrons. Two ν_μ are produced in these decays with $E_\pi/4$ energy for each photon with $E_\pi/2$. Hence, the energy in neutrinos is equal to the energy in photons [24] and $x_{\nu/\gamma} \sim 1$. In $p\gamma$ interactions 2/3 of the proton energy goes to the neutrons (protons) and the remaining third goes to the positively-charged pions (neutral pions). In the charged pion decay a single ν_μ is created with half of the pion energy for every photon with half of the neutral pion energy. Thus, in this case $x_{\nu/\gamma} \sim 4$. Table 1.1 summarises it.

Neutrino effective area

For a neutrino flux dN_ν/dE_ν at the Earth, the event rate can be computed from the "effective area":

$$R_\nu(\delta_\nu) = \frac{dN_\nu(\delta_\nu)}{dt} = \int dE_\nu A_\nu^{\rm eff}(E_\nu, \delta_\nu)\frac{dN_\nu}{dE_\nu}, \tag{1.21}$$

where $A_\nu^{\rm eff}(E_\nu, \delta_\nu)$ is the neutrino effective area, i.e. the equivalent area of a 100% efficient detector, which depends on both the neutrino energy, E_ν, and the source declination δ_ν. The neutrino effective area, which is computed via Monte Carlo simulation, takes into account the neutrino charged current cross section (see next chapter), $\sigma_\nu(E_\nu)$, the absorption of neutrinos through the Earth, $\mathrm{P_{Earth}(E_\nu)}$ and the muon detection (and selection) efficiency, ϵ, in the generation volume $V_{\rm gen}$:

$$A_\nu^{\rm eff}(E_\nu, \delta_\nu) = \epsilon \times V_{\rm gen} \times \rho \times N_{\rm A} \times \sigma_\nu(E_\nu) \times \mathrm{P_{Earth}(E_\nu)}, \tag{1.22}$$

with ρ the material density and $N_{\rm A}$ the Avogadro number. The neutrino survival probability $P_{\rm Earth}$ can be written as:

$$\mathrm{P_{Earth}} = \mathrm{e}^{-\mathrm{N_A}\sigma_\nu(\mathrm{E_\nu})\int \rho(\mathrm{l})\mathrm{dl}} \tag{1.23}$$

for a neutrino propagating through paths of density $\rho(l)$. The neutrino effective area for the ANTARES detector is shown in Figure 1.7 as a function of E_ν for three declination bands.

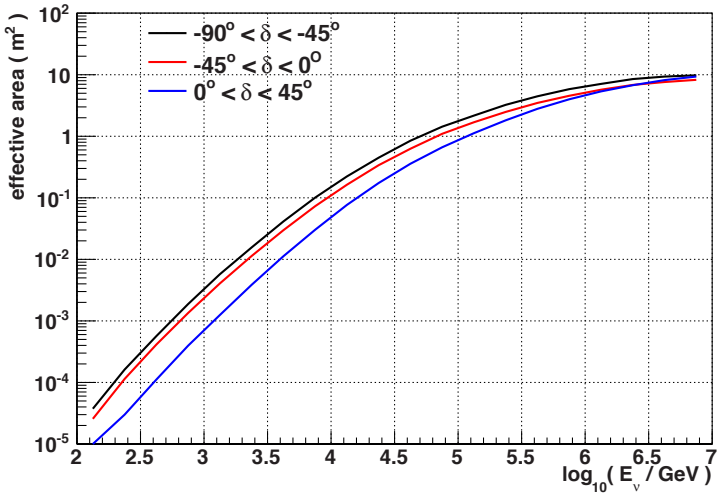

Figure 1.7.: Neutrino effective area of the ANTARES detector for the period 2007-2010 as a function of the neutrino energy for three declination bands.

1.3. Candidate sources of cosmic neutrinos

In this section possible sources of cosmic rays and neutrinos are presented. A distinction between Galactic and extragalactic sources is made. A sky-map showing the location in Galactic coordindates for some of these γ-ray sources is shown in Figure 1.9.

1.3.1. Visibility at the ANTARES site

The location of the ANTARES detector in the Mediterranean Sea makes it suitable to detect potential Galactic sources of neutrinos. Figure 1.9 shows that most of the Galactic Plane is visible for ANTARES which is sensitive to upgoing neutrinos, i.e. below the local horizon (θ <90, where θ is the zenith angle). A source at declination δ which emits neutrinos required to be as upgoing by a detector at latitude ϕ, is visible for a fraction of the day [32]:

$$f = 1 - \frac{\arccos(-\tan\delta\tan\phi)}{\pi}. \tag{1.24}$$

For example, the Galactic Center ($\delta = -29°$), which is never visible at the South Pole, has $f \approx 67\%$ at the ANTARES site ($\phi \approx 42°50'$). The SNR RX J1713.7-3946, one of the brightest TeV sources, is located at $\delta = -39.75°$ and is visible at the ANTARES site for 78% of the time. Figure 1.8 (top) shows the quantity f as a function of the detector latitude for various Galactic sources. The visibility as a function of the source declination is shown in Figure 1.8 (bottom)

1.3.2. Galactic sources

During the last decade many Galactic TeV gamma-ray sources have been discovered using atmospheric Cherenkov telescopes such as H.E.S.S. [33, 34], VERITAS [35] and MAGIC [36]. Today, the TeV source catalogue comprises more than 100 objects[5]. For many sources the question whether the observed gamma-ray flux is produced leptonically, i.e. via inverse Compton scattering, or hadronically, through the reactions described in 1.2.3, is still open.

The most promising Galactic candidate ν sources are:

- **Shell-type supernova remnants.** A supernova is a stellar explosion which ejects most of the stellar material at a velocity up to 30.000 km/s. Shock waves are generated by the interaction of the matter ejected with the interstellar medium. They could result in particle acceleration via the Fermi mechanism. The interactions of the accelerated cosmic rays with the local matter of the remnant create neutrinos and gamma-rays via decay of charged and neutral pions. Two of the most famous examples of shell-type supernova are Vela Jr.(RX J0852.04622) and RX J1713.3946-7. TeV gamma-rays have been observed from both sources [37, 38]. Predictions of neutrino emission from RX J1713.3946-7 are discussed in the next chapter.

[5] see for example the online TeV gamma-ray catalog TeVCat at http://tevcat.uchicago.edu

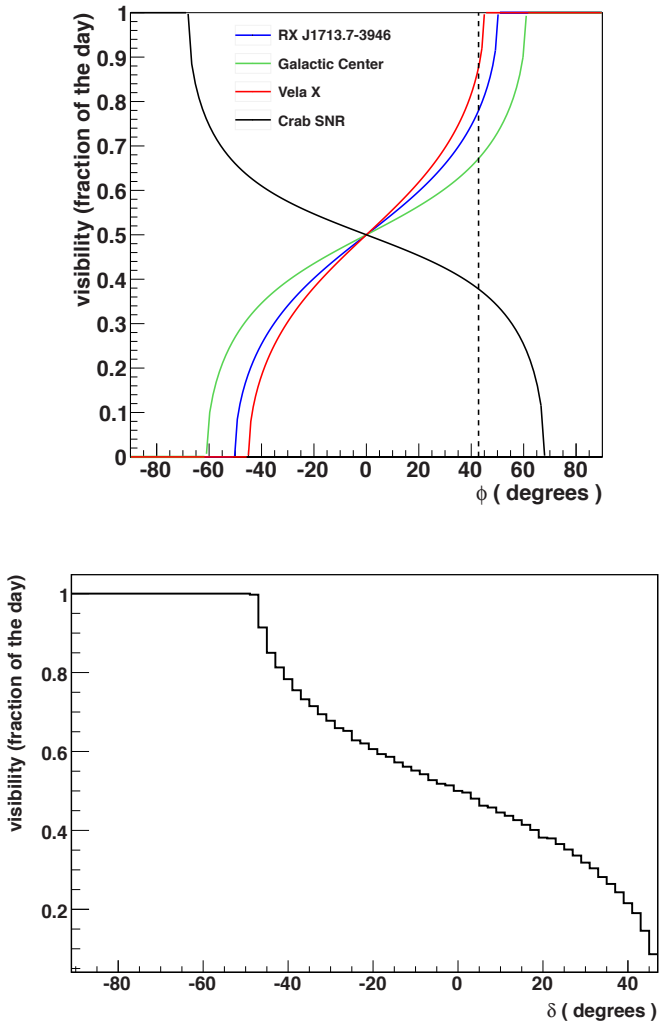

Figure 1.8.: Top: fraction of time a source is visible from a detector at latitude ϕ. The dashed line shows the ANTARES location. Bottom: visibility at the ANTARES site as a function of the source declination.

In February 2013, the Fermi-Lat [40] collaboration provided the first evidence that cosmic ray protons are accelerated in supernova remnants (SNRs) [41]. GeV gamma-rays from SNRs associated with giant molecular clouds, W 44 and IC 443, were detected. At GeV energies hadronic models fit the data better the leptonic ones. The γ-ray spectra of these two sources are shown in Figure 1.10. Both sources are investigated in the point source analysis described in this thesis.

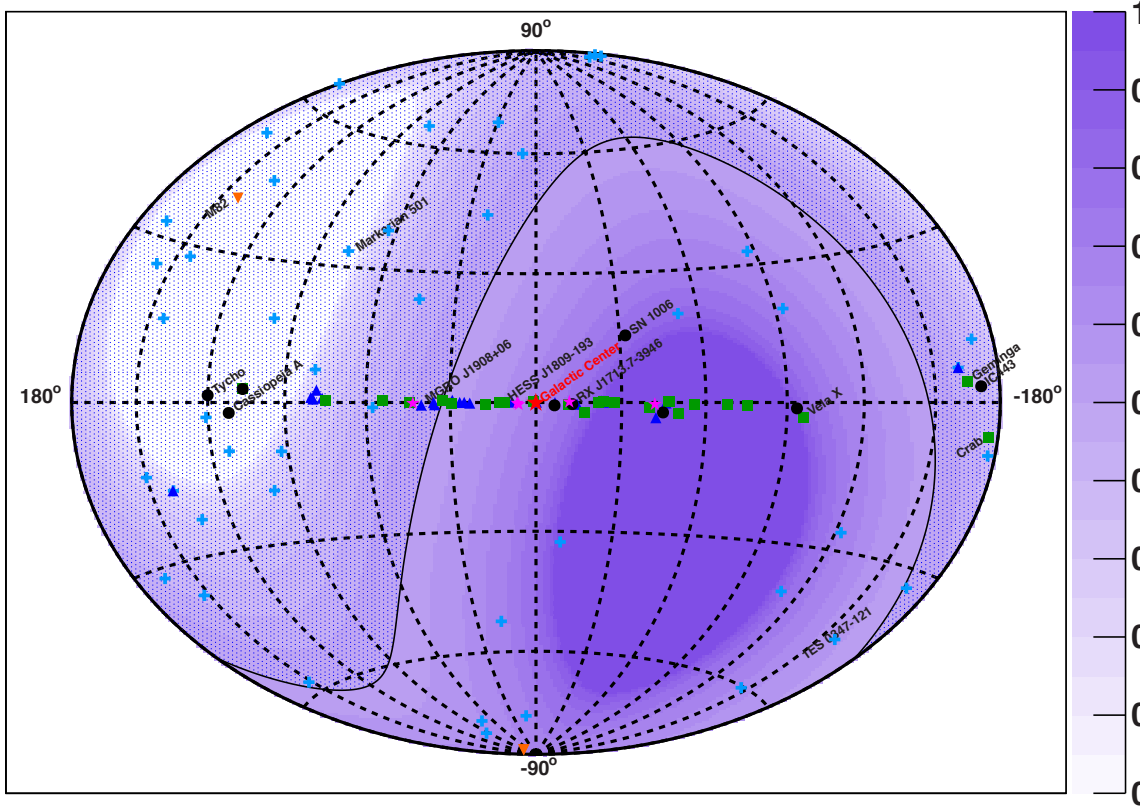

Figure 1.9.: Sky map in Galactic coordinates of TeV γ-ray sources. Different symbols represent different source types: black circles for shell type supernovae, magenta stars for supernovae remnants and molecular clouds, green squares for pulsar wind nebulae, orange triangles for starburst galaxies, blue cross for AGNs and blue triangles for unidentified sources. The red star represents the Galactic Center. The solid line shows the extend of the visibility for a South Pole detector. The visibility in ANTARES is indicated by the different shades of purple.

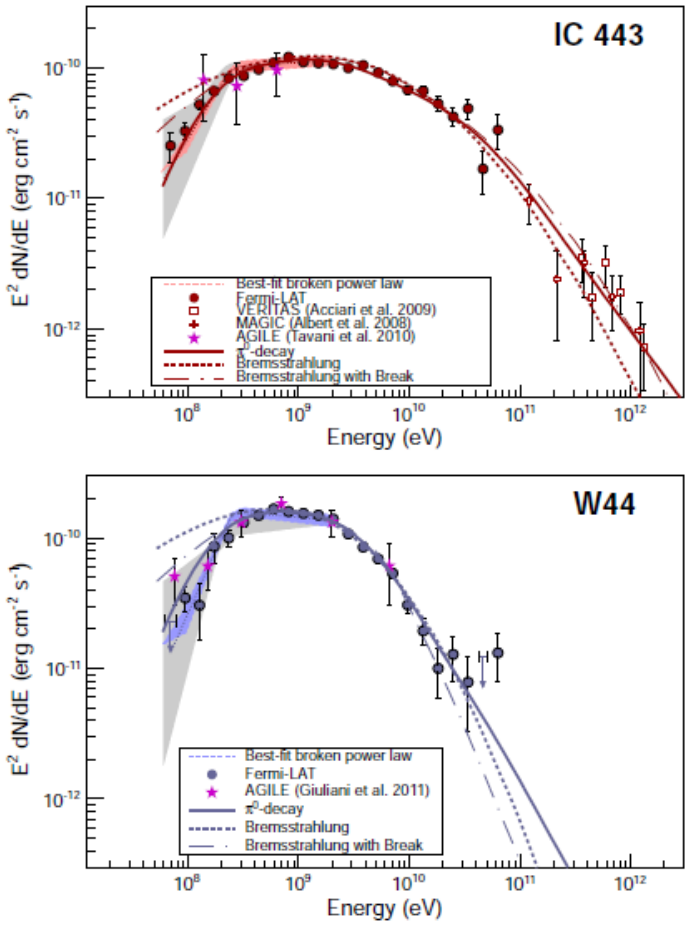

Figure 1.10.: Gamma-ray spectra of the SNRs IC 443 (top) and W44 (bottom) measured by Fermi-LAT. The solid lines denote the smoothly broken power-law function used for the fit which is based on a hadronic model. The dashed lines show the same but for a leptonic model. For IC 443 the TeV data points from MAGIC, VERITAS and H.E.S.S. are also shown.

- **Pulsar wind nebulae.** Pulsar wind nebulae (PWN), also known as plerions, are a sub-class of supernova remnants characterised by the presence of a central pulsar blowing out a "wind" of electrons and positrons into the nebula. The acceleration of cosmic rays may take place at shocks in the pulsar wind. The most famous PWN is the Crab Nebula which was the first TeV γ-ray source ever detected [39]. Another TeV γ-ray plerion is Vela X [42]. In the next chapter we will describe models of neutrino emission from these two sources.

- **Microquasars.** Microquasars are Galactic X-ray binary systems. They are usually characterised by relativistic radio jets. They consist of a compact object, such as a neutron star or a black hole, which accretes matter from a companion star usually of smaller mass. The X-ray emission can be separated into a thermal component, produced by the accretion disk, and a power law component which is generated by Compton scattering of soft photons on a gas of hot electrons. Neutrinos can be generated by the interactions of accelerated protons with synchrotron photons produced inside the jet by thermal electrons. TeV gamma-rays have been detected by H.E.S.S. for the microquasars LS 5039 [43] and LSI $+61°303$ [44]. In [45] neutrino fluxes and event rates from microquasars are predicted. The model discussed is based on the assumptions that the jets are protonic[6]. Upper limits on these models were recently obtained by the ANTARES collaboration [46].

- **Galactic center.** The H.E.S.S. telescope has observed a point-like source of very high-energy gamma rays (HESS J1745-290) [47] in the direction of the central region of our Galaxy. The source of this emission could be either the supermassive black hole Sagittarius A* or the supernova remnant (SNR) Sgr A East. Unfortunately the angular distance between these two objects is smaller than the detector angular resolution. A second observation revealed another source (HESS J1747-281) located at the same coordinates of the supernova remnant G 0.9+0.1 [48]. Recently a diffuse gamma-ray emission of energies greater than 100 GeV was discovered [49] in a very large region which spans the Galactic coordinates $|l| < 0.8°$, $|b| < 0.3°$. The measured gamma-ray flux is well described by a power lay spectrum $dN_\gamma/dE \propto (E/TeV)^{-2.29}$. Considering the morphological correlation between the high density ($n_{\rm H} \sim 10^4$ cm^3) of molecular clouds in the region and the gamma-ray emission, the only reasonable mechanism of photons production is via meson decay, thus a neutrino flux is also expected [50]. The excess of gamma-rays detected by H.E.S.S. is shown in Figure 1.11.

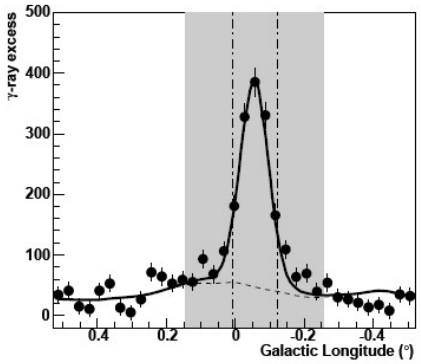

Figure 1.11.: γ-ray excess as a function of Galactic longitude. A strong emission at the Galactic center is clearly visible as well as a diffuse emission at larger longitude values. The dashed-dotted lines show the 68% containment region of the point spread function of the instrument.

- **Fermi bubbles.** The Fermi bubbles are two large bubbles extending north and south

[6] Jets dominated by electro-proton plasma.

of the Galactic center for approximately 25 thousands light years emitting gamma-rays. They were recorded for the first time in November 2010 by the Fermi-LAT detector [12]. The energy spectrum spans from 1 GeV to $\sim$ 100 GeV. Several mechanisms have been suggested in order to explain this gamma-ray emission, most of them involving leptonic processes. However, some models describe also a possible hadronic scenario via collisions of accelerated protons with a neutrino flux as consequence [51].

1.3.3. Extragalactic sources

In the following, the most promising candidate source of extragalactic neutrinos are summarised:

- **Active Galactic Nuclei.** AGN are galaxies hosting a supermassive black hole ($10^6 - 10^9$ solar masses) at their center. AGN release a large amount of energy, $L > 10^{47}\mathrm{erg/s}$, provided by the accretion of matter by the supermassive black hole. Two relativistic jets are emitted perpendicular to the accretion disk, transporting matter. A subclass of AGN is represented by the so called blazars in which the jet axis is aligned along the line of sight of an observer.

  AGNs have been observed in all frequency bands, from radio up to TeV energies.

  Many models predict neutrino emission from the relativistic jets [53, 52, 54] where the accelerated protons can interact with synchrotron photons. Protons are accelerated by shock fronts created by plasma blobs moving with different speeds. The diffuse neutrino flux predicted by these models is computed by convoluting the single source flux with the redshift and luminosity dependent number of sources, dn/dL, as:

  $$\frac{dN_\nu}{dE_\nu} \propto \int_z \int_L dL dz \frac{d\Phi_\nu}{dE_\nu}(L,z) \cdot \frac{dn}{dL}(L,z). \tag{1.25}$$

  The overall normalisation of the neutrino spectra depends on the observed gamma-ray flux. The model proposed by [53] is based on a possible correlation between the emission of X-rays and neutrinos. The prediction from Halzen and Zas [52] takes into account the results from the EGRET collaboration [64]: the diffuse extragalactic background measured by EGRET ($E_\gamma > 100$ MeV) can be interpreted as the result of interactions between TeV photons from AGNs with nucleons in the source. The normalisation of the neutrino flux proposed in [54] assumes that the neutrino emission from a single AGN is correlated to the radio luminosity.

  The flux predicted from these models has been experimentally rejected by the recent analyses from the IceCube and ANTARES collaboration [56, 57] as shown in Figure 1.14. This indicates that the assumptions made in the mode are wrong or too optimistic. For example in [54] several neutrino models from radio galaxy are discussed for different spectral shapes of the primary proton cosmic ray spectrum and optical thickness of the source. The upper limit obtained by IceCube rejects only the model with a primary cosmic ray spectrum of E^{-2} and an optical thickness $\tau = 0.2$.

- **Gamma-ray bursts.** GRBs are short but extremely energetic bursts of gamma radiation (KeV-MeV photons). The initial burst is often followed by X-ray, optical and radio emission, i.e. the so called "afterglow". GRBs are commonly divided in two categories depending on their duration. "Long" GRBs last for more than 2 seconds and have an average duration of 30 seconds while "short" GRBs last for less than 2 seconds. It is thought these correspond to different progenitors: "long" GRBs are often associated with supernovae as was first indicated by the observation of GRB980425 on April 25, 1998 and later confirmed by its coincidence in time and space with the supernova SN 1998bw [65]. "Short" GRBs are instead associated with binaries system with a small fraction of a solar mass of matter accreting on a massive black hole.

  The most widely accepted theory to describe the physics of GRBs is the "fireball" model. A "fireball", produced either during the collapse of a supernova or the merger of a binary system, expands at relativistic velocity. Cosmic rays are thought to be accelerated in the fireball internal shocks, hence neutrinos are produced in the decay of charged pions created in the interactions of protons with local photons. Two models of neutrino emission [66, 67], which assume that all UHECR are produced in GRBs, have been rejected by the IceCube collaboration [68] in a search of neutrinos from GRBs. The upper limits are a factor 3.7 below these predictions. From these results, shown in Figure 1.12, the conclusion seems that the current theories and neutrino production in GRBs have to be revisited. As a result, gamma-ray bursts are not a primary source of ultra high-energy cosmic rays.

- **Starburst galaxies.** Starburst galaxies are characterised by a very high rate of star formation often triggered by the galaxy merger mechanism. As a consequence a high rate of supernova explosions is also expected. Supernovae will therefore enrich the dense star forming region with relativistic cosmic rays accelerated in front shocks. Hence, neutrinos will be produced by the decay of charged pions generated by the interactions of relativistic protons with the interstellar medium. In [58], a flux of neutrinos from supernova remnants in starburst galaxies is predicted. The flux derived follows a power-law spectrum with an exponential cutoff. A few events per year are predicted for a kilometer scale detector. This theoretical model has been tested by a stacking search performed by the IceCube collaboration [59] using data from a partially completed detector. Upper limits have been derived.

- **Galaxy clusters.** Cluster of galaxies (GCs) are the largest gravitationally bound objects in the universe and represent a potential source of high-energy cosmic rays. Neutrinos are generated through pp interactions with the intracluster material. Neutrino fluxes for five nearby ($z < 0.03$) GCs (Virgo, Centaurus A, Perseus, Coma and Ophiuchus) are derived in [60]. The calculated event rate is shown in Figure 1.13 for a kilometer-cube detector. A few events per year are expected.

Upper bounds to the neutrino flux from Extragalactic sources

Ultra high-energy cosmic rays ($E > 10^{18}\mathrm{eV}$) are believed to have an extragalactic origin as their Larmor radius exceeds the size of the Galaxy. An upper bound to the neutrino flux

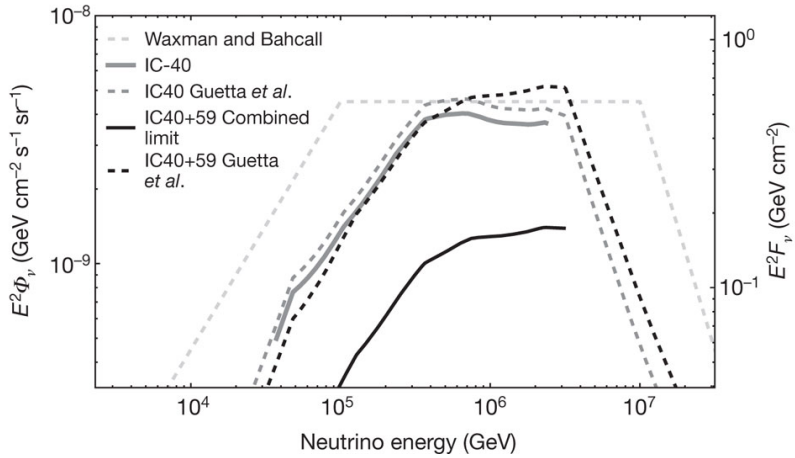

Figure 1.12.: Predictions from [66, 67] for neutrinos from GRBs are shown in dashed lines as a function of the neutrino energy. The dashed line labelled as "IC40 Guetta *et al.*" shows the flux prediction for IceCube using only 40 strings. The black dashed line labelled as "IC40+59 Guetta *et al.*" shows the prediction for the full data set of the analysis. Solid lines refer to 90% CL upper limit, with the the grey line labelled as "IC40 limit" showing the results from a previous analysis [69] and the black line labelled as "IC40+59 Combined limit" showing the final results. Figure taken from [68]

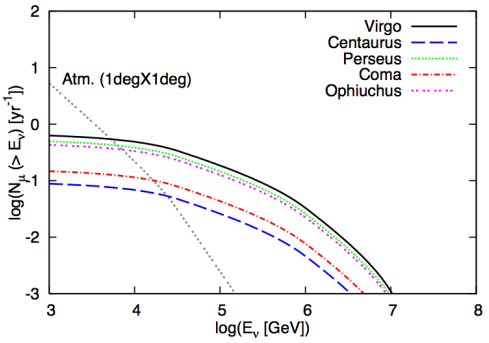

Figure 1.13: Expected event rates for muon neutrinos in a kilometer-cube detector from five GCs: Virgo, Centaurus A, Perseus, Coma and Ophiuchus. Figure taken from [60]

from extragalactic sources was estimated by Waxmann and Bahcall [61, 62]. The model applies in particular to Active Galactic Nuclei (AGNs) and Gamma-Ray Bursts (GRB) and relies on cosmic ray observations (the observed spectrum of UHECRs was used as a normalisation factor to their calculations). The upper limit is $E_\nu^2 \Phi_\nu < 4.5 \times 10^{-8} \mathrm{GeV cm^{-2} s^{-1}}$. The limit derived by Waxmann and Bahcall (WB) is based on assumptions which have been criticised [63]:

1. Neutrons generated in photohadronic interactions escape from the source.
2. Magnetic fields do not play any role in the propagation of CRs.
3. The injection spectrum is $\propto E^{-2}$.

In [63] instead, a bound has been derived directly not only from the CRs observation (as in the case of Waxmann and Bahcall) but also from the gamma-ray flux observed by EGRET [64]. The bound discussed in [63] is in general in agreement with the WB limit in the neutrino energy range $10^7 \mathrm{GeV} \leq \mathrm{E}_\nu \leq 10^9 \mathrm{GeV}$ but is higher at lower and higher energies. Both the bound predicted in [63] and by Waxmann and Bahcall are shown in Figure 1.14.

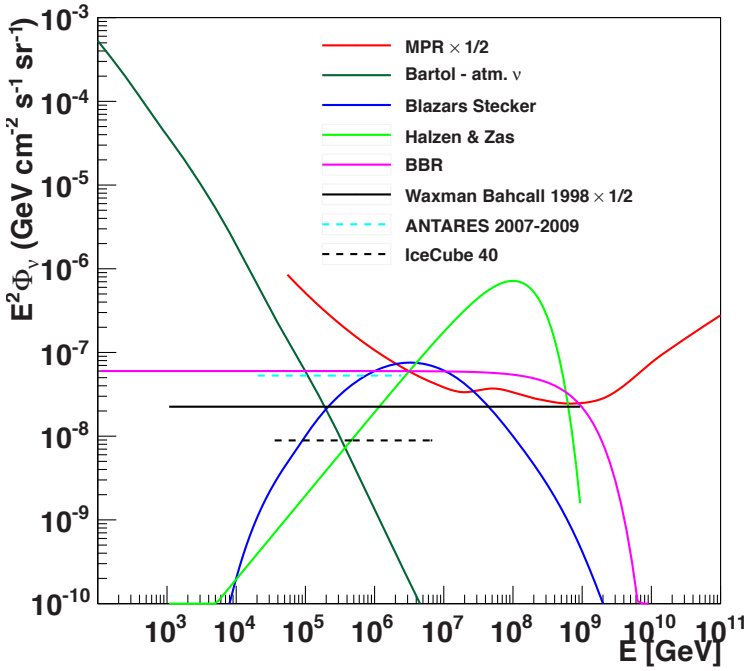

Figure 1.14.: Various predictions for the diffuse neutrino flux from AGNs together with the WB bound (solid black line) and the Mannheim, Protheroe and Rachen [63] (MPR) (solid red line). To take into account neutrino oscillations from the source to the Earth they are both divided by two. The solid green line shows the diffuse neutrino flux predicted by Halzen and Zas in 1997 [52]. The solid blue line the model by Stecker [53] for blazars and the magenta line the model by Becker, Biermann and Rhode (BBR) in 2005 [54]. The solid dark green line shows the atmospheric neutrino flux as parametrised in [55] (averaged over all ν_μ directions). Upper limits from ANTARES [57] (dashed light blue line) and IceCube [56] (dashed black line) are also shown.